

# Higher Order Recurrent Space-Time Transformer

Tsung-Ming Tai<sup>1</sup>, Giuseppe Fiameni<sup>1</sup>, Cheng-Kuang Lee<sup>1</sup>, Oswald Lanz<sup>2</sup>

<sup>1</sup> NVIDIA AI Technology Center <sup>2</sup> Fondazione Bruno Kessler

{ntai,gfiameni,cklee}@nvidia.com, lanz@fbk.eu

## Abstract

*Endowing visual agents with predictive capability is a key step towards video intelligence at scale. The predominant modeling paradigm for this is sequence learning, mostly implemented through LSTMs. Feed-forward Transformer architectures have replaced recurrent model designs in ML applications of language processing and also partly in computer vision. In this paper we investigate on the competitiveness of Transformer-style architectures for video predictive tasks. To do so we propose HORST, a novel higher order recurrent layer design whose core element is a spatial-temporal decomposition of self-attention for video. HORST achieves state of the art competitive performance on Something-Something-V2 early action recognition and EPIC-Kitchens-55 action anticipation, without exploiting a task specific design. We believe this is promising evidence of causal predictive capability that we attribute to our recurrent higher order design of self-attention.*

## 1. Introduction

Recognizing human actions from videos is a long-standing and widely studied problem in computer vision. Most work has addressed action recognition as a video clip classification problem, lately almost exclusively with deep learning approaches, and a steady progress has helped to push the limits of spatio-temporal feature learning from video. An underlying assumption in action recognition as clip classification is that of complete and synchronous observation, that is, the action to be recognized is immediately accessible and entirely represented in the video clip. Such completeness assumption no longer holds with video prediction tasks, which are to forecast the future from partial observations of the past. Also, in practical setting observations may be streamed and thus elaborated progressively to perform and revise future prediction continuously over time. These are requirements shared among many real world applications of video based human prediction, e.g. in human-robot collaboration, real-time video surveillance,

and autonomous driving.

We illustrate the problem setting of early action recognition and action anticipation in Fig. 1. As opposed to recognition, both require prediction of action labels beyond the extend of the observed video sub-clip. In early recognition, the target label is global and the action is already represented, even if not to its full extent, as signal in the sub-clip. In anticipation, the target action only stays in causal relation to the signal in the sub-clip, but is not directly observable in it. It must be forecast as one possible consequence of the observed. While a clip classification design could be deployed for prediction, such approach would not take advantage of these peculiar challenges that are not necessarily relevant for recognition. The problem to solve is different.

A standard modeling framework for anticipation and early recognition is recursive sequence prediction [1, 2, 3], where video frames are consumed in sequence to progressively update a representation of the relevant video content. The working assumption is that recursive updating better aligns with causality and can promote short-term predictive learning. Recent work has expanded upon LSTM or GRU design to realize models capable of capturing higher order correlations across time [1], that fork parallel models at each iteration to simultaneously update a representation of the past while predicting the future with an encoder-decoder approach [2], and revise intermediate representations through a dynamic re-weighting mechanism in a self-regulated learning framework [3]. The shared objective of these works is to mitigate performance degradation due to accumulation of anticipation error. Some works furthermore attempt to tame the uncertainty induced by longer anticipation time through predicting multiple futures [4] and enforce their causality through cycle consistency [5].

In this paper we explore on the design and effective learning of space-time transformers for predictive tasks such as early recognition and anticipation. Transformers have replaced recurrent models in ML applications of language processing and also partly in computer vision. Latest work demonstrates that convolution-free, pure transformer architectures can compete with video CNNs on action classification [6, 7]. Timely enough, in this paper we investigate

whether they can replace LSTMs on video predictive tasks, where LSTMs are still the common modeling paradigm of best performing methods. To verify this, we propose a novel higher order recurrent layer whose core element is a spatial-temporal decomposition of self-attention for video. It is higher order as it maintains a state queue in the attention mechanism to keep track of previously recorded information. It is recurrent in the way the queue is updated at each time step. Our layer is lightweight and has a transparent design, and achieves state of the art competitive performance without bells and whistles when deployed for early action recognition and anticipation. Competitors explicitly unfold over anticipation intervals to predict the future while in our evaluation we do not (yet) leverage such task-specific design. We believe this is promising evidence of causal predictive capacity that we attribute to our recurrent higher order design of self-attention.

## 2. Related work

Our work is related to past research on video action recognition, early action recognition and activity anticipation.

### 2.1. Action Recognition

Classic approaches to action recognition extract hand-crafted features from video and train a classifier on these to solve the task [8, 9]. Modern approaches blend feature extraction and classification into modular, end-to-end trainable neural architectures that can effectively learn from larger and larger datasets, and consequently, generalize better. Building on the success of 2D CNNs for image recognition, early approaches use temporal pooling of frame-level features to process video as a set of images [10, 11] or use two-stream architectures to fuse frame features with features extracted from optical flow [12, 13]. 3D CNNs process videos in space-time by expanding 2D kernels along the temporal dimension [14, 15, 16], requiring more parameters and compute. Learning spatio-temporal features with less is a common objective of many recent works. These include decomposing 3D convolutions into 2D spatial followed by 1D temporal [17], replacing 1D with hard-coded time shifts [18] or learnable gating [19], decompose channel dimensions using group convolutions [20], modeling interactions between separated dimensions [21], and through adaptive fusion [22]. Sequence learning models based on LSTM have been augmented with attention to perform well on action recognition [23, 24, 25]. Transformer inspired attention layers [26] have been introduced in video CNNs [27, 28, 29], and a recent study demonstrates that pure self-attention based, convolution-free architectures can compete in action recognition [6, 7].

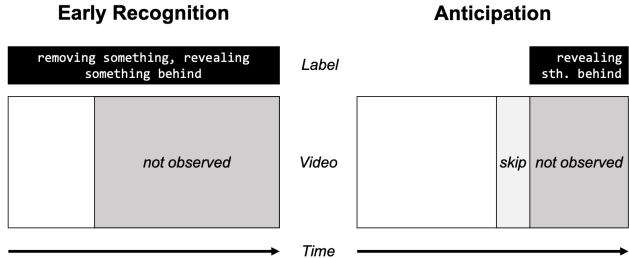


Figure 1: **Early Recognition vs Anticipation.** In early recognition the action can be partially observed, in anticipation it can only be inferred as a consequence of the observed.

### 2.2. Early Action Recognition

Works on this topic often expand upon action recognition architectures. Using a video classifier trained on sub-clips is often utilized as a baseline, which is valid in early recognition since the target action is already observed in the sub-clip. Given the nature of problem that is to predict from an initial part of a frame sequence, a most intuitive framework can be that of recurrent models such as LSTMs. LSTM architectures can be trained under the assumption that recognition confidence should be non-decreasing as the model observes more of the action by introducing a ranking loss [30]. Following a same assumption, a multi-stage LSTM architecture integrating context-aware and action-aware is trained with a loss that encourages to make correct predictions as early as possible in the input sequence [31]. Sequential context can be leveraged to reconstruct missing information in the features extracted from partial video by learning from fully observed action videos [32]. LSTMs are the building blocks of a two-stream feedback network where one stream processes the input and the other models the temporal relations to promote the representation of temporal dependencies [33]. Eidetic LSTM [34] introduce an attentive mechanism to memorize local appearance or short-term motion, and use it to improve predictive spatio-temporal feature learning. A higher order LSTM with convolutional gates uses multiple inputs from the past to update its internal state [1]. Using tensor train decomposition, their extension effectively dominates compute and parameter count to grow at most linearly in time and space.

### 2.3. Activity Anticipation

Differently from early recognition, anticipation is to predict the action from observations before it actually starts. The problem has been studied in the context of third person vision but recently also with major efforts in robotic and egocentric, first person vision due to applications in human-robot interaction, assistive technology and au-

onomous driving. Early work combines a Markov decision process model with ideas from control theory to forecast human trajectories using semantic scene context [35]. [36] proposes a CRF learning framework which integrates object affordances to inform about possible future actions. [37] addresses action anticipation by training a CNN to regress the representations of future frames from past ones in an unsupervised way. A encoder-decoder LSTM network is presented in [38] which takes multiple past representations as input and learns to anticipate a time series of future representations. [39] investigate on the use of CNNs and GRUs to learn future video labels based on previously seen content. An anticipatory model is combined with an auxiliary model to take into account possible actions and scene attributes and to reason about how they may evolve over time [40]. RU-LSTM [41] is a learning architecture which processes RGB frame snippets, optical flow and object features using two LSTMs and modality attention to anticipate future actions. The two LSTMs behave like an encoder-decoder, where the first progressively summarizes the observed together with the second that unrolls over future predictions without observing. A self-regulated learning framework for activity anticipation in egocentric video is presented in [42], that utilizes LSTMs to progressively re-weight previously observed content, and to rectify predicted intermediate representations. The spatio-temporal graph transformer in [43] tackles trajectory prediction by only attention mechanisms.

**Conclusion.** Compared to these existing works, and to the best of our knowledge, we provide the first study on Transformer-style architectures for video prediction tasks. Our spatial temporal decomposition of self-attention in Sec. 3.2.1 is custom design and has no trivial grounding in existing work. Transformers were introduced to eliminate recurrence in the LSTM dominated language processing, while this work is the first to blend the two, via a state queue management internal to space-time self-attention which makes it higher order.

### 3. Recurrent Space-Time Transformers

We present our sequential prediction framework for early recognition and anticipation from video.

#### 3.1. Higher Order Prediction Framework

An overview of our framework is presented in Fig. 2. At each time step  $t$ , we transform a feature representation  $x(t)$  of the current frame through higher order spatial-temporal filtering layers. To do so, each such layer maintains a queue  $H(t) = [H_{t-1}, \dots, H_{t-S}]$  to keep track of  $S$  previous states, and combines them to produce an updated representation  $y(t)$  as output,

$$y(t) = F(x(t), \Phi(h(t), H(t))) \quad (1)$$

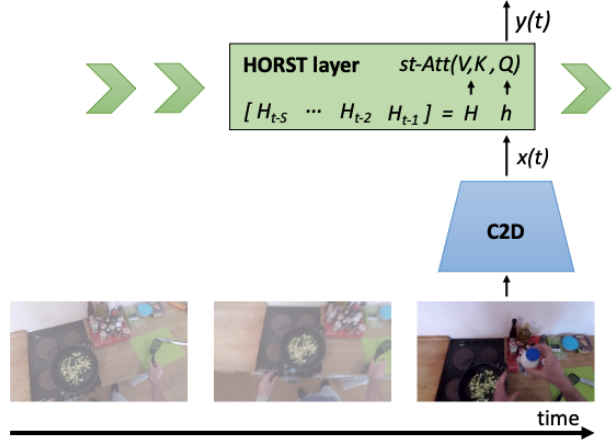


Figure 2: **Higher Order Recurrent Space-Time Transformer (HORST).** Our framework leverages a spatial-temporal recurrent self-attention to incorporate higher order correlations for prediction, by maintaining a queue of states to keep track of previously recorded information.

States  $H$  are put in place to enable  $F$  incorporate high order correlations among a transformed version  $h$  of the layer input  $x$  and a representation of previously recorded information. The aggregation function  $\Phi$  hereby plays a key role for our model to realize feature transformations that are effective for video prediction tasks. We identify the following desired properties that support our design choices.  $\Phi$  should

- provide selective access to spatially local information from the past, in order to promote those locations in each latent state that correlate with the most prominent features in current input, and filter out the irrelevant;
- diversify the importance of each state in the temporal aggregation, in order to promote contributions of states based on global, as opposed to spatially local, information from the input;
- have few parameters, in order to push most of learning capacity to the feature transform  $F$  and propagate strong learning signal down for input feature learning.

We now present a novel self-attention to realize  $\Phi$ , whose design is inspired by these identified properties.

#### 3.2. Space-Time Transformer Layer

To distill the information from the past that is relevant to the current input, we employ dot-product self attention with the input as query and the state queue as keys and values. That is, given learnable embeddings (for notation convenience we omit reference to time  $t$  from now on)

$$Q, K, V = \omega(h), \phi(H), \psi(H) \quad (2)$$

with parameters  $\theta_\omega, \theta_\phi, \theta_\psi$ , we compute query-key correlations, normalize with scaled softmax and apply as weights to aggregate the values ( $C$  is number of query channels),

$$Att(Q, K, V) = softmax(Q^T K / \sqrt{C}) V \quad (3)$$

We now show how we arrange self-attention in space and time to obtain  $\Phi$ .

### 3.2.1 Spatial-Temporal Attention

Trivially applying Eq. (3) to model the aggregation function  $\Phi$  in (1) incurs in the following. Joint space-time attention requires  $(HW)^{S+1}$  pixel level key-query comparisons (dot-products between vectors of size  $C$ ), and may result over fine-grained as the correlations are found at pixel granularity. The opposite is flattening query and keys which leads to full-temporal attention,  $S$  dot-products among vectors of size  $HW C$  are computed to obtain the weights to apply on  $V$ . However, values  $V$  about objects and scene context may be hard to distill with a global query-key comparison, but these can be the information to use for prediction.

We propose a new design of space-time attention to addresses both issues, granularity and complexity. We approximate joint  $H \times W \times S$  attention using rank-1 decomposition

$$st-Att(Q, K, V) = (\mathcal{T}(Q, K) \otimes \mathcal{S}(Q, K)) V \quad (4)$$

where  $\mathcal{T}, \mathcal{S}$  are temporal  $1 \times S$  and spatial  $H \times W$ . To define spatial and temporal, we introduce spatial filter maps  $f_K, f_Q$  for keys and query. Their role is attending the relevant spatial regions in keys and query. We use the following

$$f_X(X) = sigmoid(\theta_X * [X_{max}, X_{avg}]) \quad (5)$$

where  $X_{avg}, X_{max}$  are channel mean and max pooled,  $\theta_K, \theta_Q$  are convolution kernels and  $sigmoid$  is to map to range [0:1]. We use  $f_K, f_Q$  as weight maps to filter keys and query for space-time attention computation with spatial temporal design defined as

$$\mathcal{S}(Q, K) = sigmoid(sap(f_K(K) \cdot Q)^T K) \quad (6)$$

$$\mathcal{T}(Q, K) = softmax(1 / \sqrt{HWC} (f_Q(Q) \cdot Q)^T (f_K(K) \cdot K)) \quad (7)$$

where  $sap$  is mean pooling over spatial.

The design choices for spatial temporal decomposition are motivated as follows. For  $\mathcal{S}$  we extract  $S$  spatially filtered queries from  $Q$ , which summarize the  $S$  regions of  $Q$  promoted independently by each of the keys through  $f_K(K)$ . This provides  $S$  pixel level queries to apply on  $K$  through (6), which can represent different regions of  $Q$  belonging to objects or scene features promoted by the keys. The correlations computed through (6) are therefore at the granularity of  $f_K(K)$  which can vary from pixel level (as

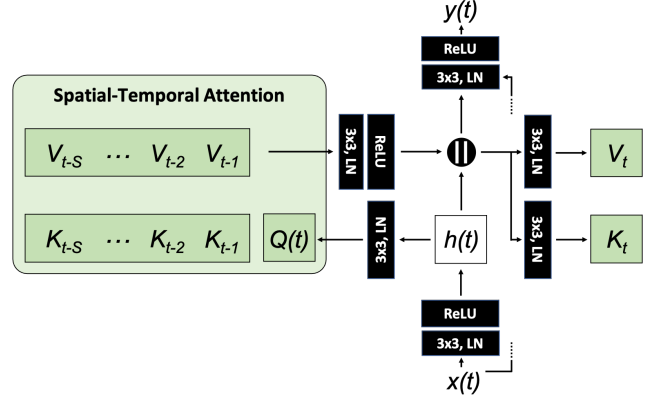


Figure 3: **Space-Time Transformer layer** (sequential implementation). Through concatenating the input transform with the output of attention operation in the key-value queue management, a recurrence of order  $S$  is introduced.

for joint spatio-temporal, by a strong filter response from  $f_K$ ) to global (as for full-temporal attention, by a uniform response of  $f_K$ ). We use  $sigmoid$  instead of normalization through scaled softmax to promote strong diverse responses for spatial decomposition. For temporal  $\mathcal{T}$  in (7) instead, we apply the self filtered global query  $f_Q(Q) \cdot Q$  on the self filtered global keys  $f_K(K) \cdot K$  using  $scaled\ softmax$ . This way we attribute a relative importance to each value in the queue using spatially filtered global query-key comparisons. With these complementary design choices, spatial-temporal decomposition in (4) can selectively utilize and integrate in a complementary way diverse information in keys and query extracted through the learnable spatial filters  $f_K, f_Q$ .

### 3.2.2 Layer Implementation

Following our spatial-temporal design of Eq. (4),  $\mathcal{T}(Q, K)$  and  $\mathcal{S}(Q, K)$  are computed in parallel from embeddings  $Q = \omega(h(t))$  and  $K = \phi([H_{t-1}, \dots, H_{t-S}])$ , and combined into a rank-1 space-time attention tensor  $\mathcal{T} \otimes \mathcal{S}$  that is applied on  $V = \psi([V_{t-1}, \dots, V_{t-S}])$ . Each embedding is a Conv, LayerNorm block. We obtain  $h(t)$  from the layer input  $x(t)$  using Conv, LayerNorm, ReLU block and apply a same block design to transform the output of spatial-temporal attention and also at the layer output, see Fig. 3. In our implementation we do not queue states, but key and values. To update their queues, we concatenate the transformed attention output with  $h(t)$ , apply the embeddings and push them to the queues (and pop the elements from position  $S$ ). Note that by concatenating  $h(t)$  with attention output, the new  $K_t$  depends on  $K_{t-1}, K_{t-2}, \dots$ , which introduces recurrence of order  $S$  into spatial-temporal attention. We add a skip connection from layer input to output transform. A recent study has shown that skip connections



are necessary to prevent rank collapse in training attention architectures [44].

Our layer is lightweight, see Tab. 1. It has 8 kernels for  $3 \times 3$  convolutions: three for embedding ( $\theta_\omega, \theta_\phi, \theta_\psi$ ), three for input-output transforms with ReLUs ( $\theta_x, \theta_v, \theta_y$ ), and two for spatial key-value filtering ( $\theta_K, \theta_V$ ). The dominant compute is key-value comparison, which depends on the order  $S$ , the spatial resolution  $HW$ , and the channel dimension  $C$ . Our spatial-temporal decomposition requires  $HWS$  dot-products between vectors of size  $C$  for spatial plus  $S$  between vectors of size  $HWC$  for temporal, which is  $HWS \times C + S \times HWC$ . This is far less than joint spatio-temporal  $(HW)^{S+1} \times C$ , and approximately twice of full-temporal  $S \times HWC$  while being more fine-grained.

Table 1: Number of parameters and multiplicative operations (MulOps) for each transformation in our layer. (normalization modules and activation functions are ignored)

Modules	Parameters	MulOps
$x_t$ to $h_t$	$C_{in} \times C_{in} \times 3 \times 3$	$9C_{in}^2 HW$
$\omega$	$C_{in} \times C_{in} \times 3 \times 3$	$9C_{in}^2 HW$
$\phi$	$2C_{in} \times C_{in} \times 3 \times 3$	$18SC_{in}^2 HW$
$\psi$	$2C_{in} \times C_{in} \times 3 \times 3$	$18SC_{in}^2 HW$
$f_Q$	$2 \times 1 \times 3 \times 3$	$18HW$
$f_K$	$2 \times 1 \times 3 \times 3$	$18SHW$
<i>st-Att</i>	-	$(6S + 1)CHW$
Post <i>st-Att</i>	$C_{in} \times C_{in} \times 3 \times 3$	$9C_{in}^2 HW$
$F$ in Eq. (1)	$3C_{in} \times C_{out} \times 3 \times 3$	$27C_{in}C_{out}HW$

## 4. Experiments

We provide short descriptions of datasets used for experimental validation, report on implementation details and training protocol to ensure reproducibility, analyze design choices of our model, and discuss obtained results.

### 4.1. Datasets

**Something-Something (SSv2).** SSv2 [45] is a large collection of action video clips with duration ranging from 2 to 6 seconds, recorded at 24 frames per second (fps). In our experiments we follow the data split scheme introduced by the dataset developers with a subset of 41 categories. There are 56769 video clips for training and 7503 for validation. Early action recognition setting is adopted where the model predicts the target action category by observing the first 25% or 50% of frames of the action clip. We use Top-1 accuracy to measure model performance.

**EPIC-Kitchens (EK55).** EK55 [46] is a large scale ego-centric video dataset containing 39596 action (verb-noun pair) annotations from 125 verbs and 352 nouns. Videos are captured by 32 subjects in 32 different kitchens. The public

training set is with 23492 action segments, and 4979 segments for validation. All unique verb-noun pairs are considered to be the categories of actions, resulting in a total 2513 action categories. Top-5 accuracy of actions across a range of anticipation times is commonly used as the metrics to measure model performance. Accuracy and class-aware Top-5 mean recall [47] for noun, verb, and action predictions at 1s are also considered for performance comparison.

### 4.2. Implementation Details

**Sampling.** For SSv2, inputs are resized to 224x224 and kept with 24 fps, and only the first 25% or 50% are used for training and testing. Note the inputs are not re-sampled to a fixed numbers of frames for each video clip segment, thus inputs are processed every 0.25 seconds. In our setting the model can observe 6 frames, and perform the anticipation with  $\tau_a \in \{2, 1.75, 1.5, 1.25, 1, 0.75, 0.5, 0.25\}$  seconds before the actual start time of the target action.

**Architecture.** For SSv2 we stack two 3x3 convolutional layers with 128 filters and stride 2 to downscale the inputs to 56x56, and add 4 HORST layers, with stride of the last two layers set to 2. We shrink the outputs to 14x14 and feed them through a classifier composed of a convolutional layer and global averaging pooling followed by a fully-connected layer to map the action categories. For EK55 we adopt BN-Inception [48], and used the same pretrained weights as [41]. We input RGB frames of size 256x454 and use the 8x14 feature maps before the global average pooling layer as input to our bottom layer. We average pool the final layer outputs and classify with a fully connected layer.

**Training.** For all experiments in this paper, RandAugment [49] is applied as augmentation scheme. We use AdBelief [50] in combination with look-ahead optimizer [51]. Weight decay is set to 0.001. Learning rate is fixed to a high ratio, 0.002, and we switch to cosine annealing down to 0 for the last 25% of epochs. We set the total training epochs to 50 for all experiments. We use  $4 \times$  NVIDIA V-100 32G GPUs for training. Batch size is set to 8 for early recognition on SSv2 and to 32 for anticipation on EK55.

**Code.** We provide a PyTorch implementation at <https://github.com/CorcovadoMing/HORST>.

### 4.3. Model Analysis

We provide a model analysis on SSv2 early recognition to explore how different design choices impact on model performance. Based on this analysis, we decide on the final model configuration for our comparative experiments.

Tab. 2 shows the performance using different design choices of space-time attention. To perform this analysis we use a stack of 4 layers and evaluate on 25% early recognition setting. By using temporal only ( $\mathcal{T}$ , Eq. (7)), we obtain 32.7% Top-1 accuracy. By reverting all layers to spatial only ( $\mathcal{S}$ , Eq. (6)) a 1.5% performance drop is ob-

Table 2: Model analysis on spatial temporal attention design.

Method	Accuracy (%)
4 × Temporal only	32.7
4 × Spatial only	31.2
4 × Spatial-Temporal	33.9
2 × Spatial-Temporal	32.2

Table 3: Model analysis on the impact of the model order,  $S$ .

Methods	Accuracy (%)
Order-1	30.7
Order-3	31.2
Order-8	33.9

Table 4: Model analysis on different choices for key and value.

Method	Accuracy (%)
$st-Att \rightarrow K; h \rightarrow V$	30.6
$st-Att, h \rightarrow V, K$	33.9

served, which is in expected for temporally-heavy datasets like SSV2. Combined spatial temporal yields the best result, 33.9%, showing that our decomposition scheme is well calibrated to attend the relevant information in the data. We also report the accuracy improvement obtained by increasing the number of stacked layers from 2 to 4, indicating that the representation in each layer is stable and further leveraged in the deeper architectural design.

In Tab. 3 we report results by varying the order,  $S$ , of HORST. Note that order corresponds to number of states in the queue where spatial-temporal attention can query. A higher order will expose a longer history of past states to the attention computation. By setting the order to  $S = 1$ , our model collapses to the Markov recurrent assumption, and the previous state will always be selected from temporal attention. The order-3 option is the default setting of Conv-TT-LSTM [1] used throughout their study. Authors reported using higher orders caused the model training to suffer from gradient instability. However, and in contrast to Conv-TT-LSTM, our spatial-temporal design directly distributes the gradient flow to the selected states. This motivated us to move on much higher order without observing training instability. We found order-8 to further boost the performance from 31.2% to 33.9%, which is 2.7% higher than using order-3. These results show that higher order can effectively be leveraged by spatial-temporal attention, and reflect favourably on Top-1 accuracy.

Finally, in Tab. 4 we report on the performance comparison of using two different options to route information to

Table 5: Something-Something 25% early action recognition results. (\*) indicates reproduced by us using our training protocol.

Methods	Accuracy (%)
3D-CNN	13.3
E3D-LSTM [34]	14.6
ConvLSTM	15.5
Conv-TT-LSTM [1]	19.5
Conv-TT-LSTM* [1]	29.3
HORST (Ours)	33.9

Table 6: Something-Something 50% early action recognition results.

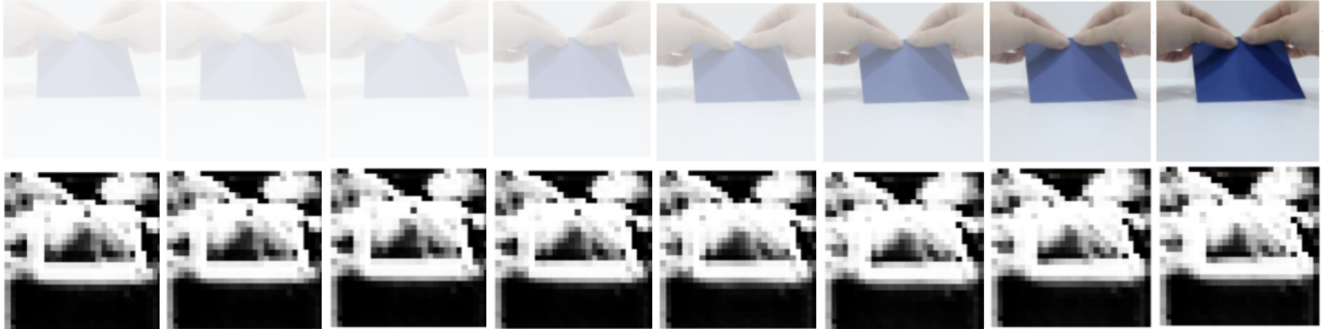
Methods	Accuracy (%)
3D-CNN	20.7
E3D-LSTM [34]	22.7
ConvLSTM	22.0
Conv-TT-LSTM [1]	30.1
HORST (Ours)	47.8

the state queue for spatial-temporal attention. The design in Fig. 3 uses the concatenated  $[h(t), st-Att]$  to produce both  $K_t$  and  $V_t$ . An alternative is to use  $h(t) \rightarrow V_t$  and  $st-Att \rightarrow K_t$ . We evaluate both options, and a large performance drop is observed when using the second. An interpretation is the following.  $st-Att$ , due to  $\mathcal{T}$ , will aggregate past values  $V$  with different associated weights. At a next time step, the distribution of weights may change and therefore,  $st-Att$  will aggregate differently. This causes key-value misaligned in time, explaining the performance drop. Binding  $st-Att$  and  $h_t$  (which is directly encoded from the layer input  $x(t)$ ) instead, would mix their complementary information to form a rich representation for keys and values. Indeed, this leads to a 3.3% improvement of Top-1 accuracy for 25% early action recognition.

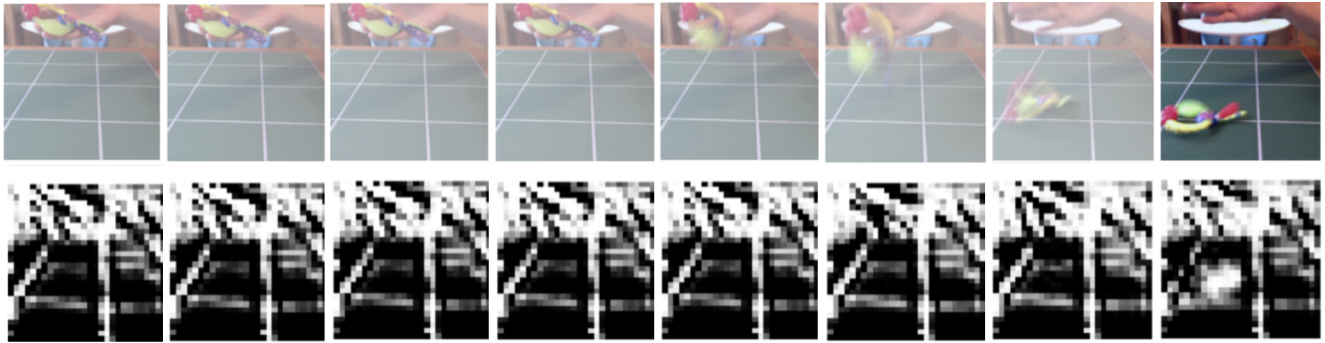
#### 4.4. Early Action Recognition on Something-Something

Tab. 5 compares Top-1 accuracy of HORST with other state-of-the-arts methods for 25% early action recognition on SSV2. We also reproduced Conv-TT-LSTM [1], the best performing competitor, using their implementation and our training protocol and architecture design for the purpose of fair comparison. Our method outperforms all previous methods by a notable margin, leading to +4.6% absolute improvement over Top-1 accuracy to Conv-TT-LSTM, which also enjoys a higher order design.

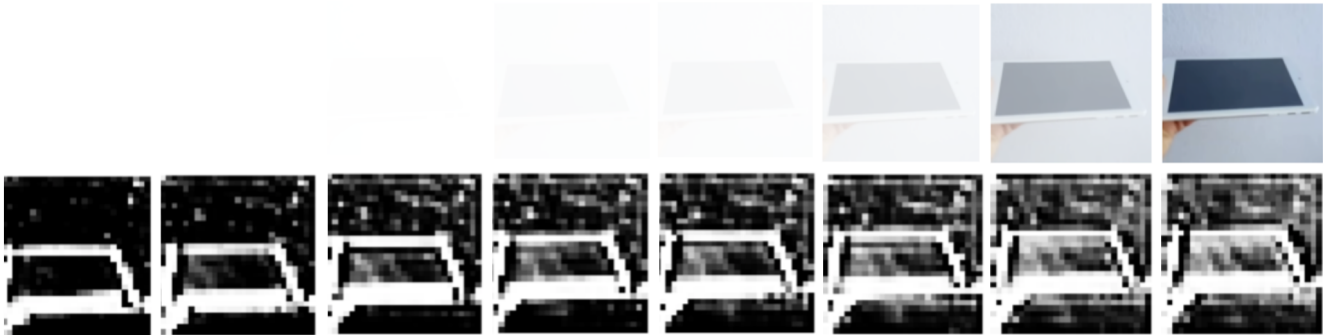
Tab. 6 shows the Top-1 accuracy using the 50% early action recognition configuration on SSV2. We report a significant gain over previous state-of-the-art methods by a large margin. It reveals the effectiveness of spatial-temporal at-



(a) Tearing [something] into two pieces.



(b) [Something] falling like a rock.



(c) Moving [something] up

Figure 4: Visualization of the results of  $\mathcal{T}$  and  $\mathcal{S}$  learned from Eq (4). The horizontal axis contains 8 frames ordered by the occurrence time from left to right. Each example comes with two rows: the upper rows are the input frames weighted by  $\mathcal{T}$ ; the bottom rows show the corresponding  $\mathcal{S}$  maps. The caption of each figure reveals its label.

tention design with higher order feature integrated, leading to a +17.7% absolute Top-1 accuracy improvement.

Fig. 4 shows examples of visualization results of temporal and spatial weighting,  $\mathcal{T}$  and  $\mathcal{S}$  defined in Eq. (4). The horizontal axis contains eight frames ordered by occurrence time from left to right. Each example comes with two rows: the top row shows the input frames weighted by  $\mathcal{T}$ ; the bottom row shows the corresponding spatial maps  $\mathcal{S}$ . Fig. 4a shows a sample labeled with *Tearing [something] into two pieces*, it can be observed that spatial attention focuses on the border of the object and on both hands, in order to predict the *Tearing* action. Temporal information shows rea-

sonable increasing focus from past to recent. The example in Fig. 4b has label *[Something] falling like a rock*, spatial attention monitors the entire environment and captures the object in the last frame. We can see that temporal weighting is uniformly distributed over the past 7 frames but suddenly increases its curiosity on the last frame to observe the event. Fig. 4c shows an action example with label *Moving [something] up*. Based on the weight map produced from spatial attention, the border of object is highlighted with the object movement, and can be clearly associated with a "moving up" action. Temporal attention in this case only focuses on the few recent frames in order to capture the relevant fea-

Table 7: EPIC-Kitchens Action Anticipation results. ( $\dagger$  is with pre-trained weights from [52])

Methods	Top-5 Accuracy % at different $\tau_a$								Top-5 Acc. % @ 1s			Mean Top-5 Rec. % @ 1s		
	2	1.75	1.5	1.25	1.0	0.75	0.5	0.25	Verb	Noun	Action	Verb	Noun	Action
DRM [53]	-	-	-	-	16.86	-	-	-	73.66	29.99	16.86	24.50	20.89	03.23
ATSN [46]	-	-	-	-	16.29	-	-	-	77.30	39.93	16.29	33.08	32.77	07.06
MCE [47]	-	-	-	-	26.11	-	-	-	73.35	38.86	26.11	34.62	32.59	06.50
VN-CE [46]	-	-	-	-	17.31	-	-	-	<u>77.67</u>	39.50	17.31	34.05	34.50	07.73
SVM-TOP3 [54]	-	-	-	-	25.42	-	-	-	72.70	28.41	25.42	<b>41.90</b>	34.69	05.32
SVM-TOP5 [54]	-	-	-	-	24.46	-	-	-	69.17	36.66	24.46	40.27	32.69	05.23
VNMCE+T3 [47]	-	-	-	-	25.95	-	-	-	74.05	39.18	25.95	40.17	34.15	05.57
VNMCE+T5 [47]	-	-	-	-	26.01	-	-	-	74.07	39.10	26.01	41.62	35.49	05.78
ED [38]	21.53	22.22	23.20	24.78	25.75	26.69	27.66	29.74	75.46	42.96	25.75	<u>41.77</u>	42.59	<b>10.97</b>
FN [33]	23.47	24.07	24.68	25.66	26.27	26.87	27.88	28.96	74.84	40.87	26.27	35.30	37.77	06.64
RL [30]	<b>25.95</b>	<b>26.49</b>	<u>27.15</u>	<u>28.48</u>	29.61	30.81	<u>31.86</u>	32.84	76.79	44.53	29.61	40.80	40.87	10.64
EL [55]	24.68	25.68	26.41	27.35	28.56	30.27	<u>31.50</u>	<b>33.55</b>	75.66	43.72	28.56	38.70	40.32	08.62
HORST (Ours)	24.68	26.03	27.09	28.40	<u>29.95</u>	<u>30.83</u>	<u>31.86</u>	32.92	<b>77.74</b>	<u>46.00</u>	<u>29.95</u>	38.38	<b>45.22</b>	10.25
HORST (Ours, 2 layers)	<u>25.38</u>	<u>26.37</u>	<b>27.82</b>	<b>29.16</b>	<b>30.69</b>	<b>31.54</b>	<b>32.52</b>	<u>33.45</u>	<u>77.67</u>	<b>46.34</b>	<b>30.69</b>	36.54	<u>44.33</u>	<u>10.94</u>
RU-RGB [41]	25.44	26.89	28.32	29.42	30.83	32.00	33.31	34.47	-	-	30.83	-	-	-
$\Delta$ (%)	-0.06	-0.52	-0.50	-0.26	-0.14	-0.46	-0.66	-1.02	-	-	-0.14	-	-	-
HORST $\dagger$ (Ours, 2 layers)	30.81	32.22	33.31	34.55	36.56	38.23	39.08	41.43	80.19	54.79	36.56	45.26	55.01	13.90

tures that allow to distinguish the action among all possibilities. Note the spatial and temporal attentions are calculated and applied to value in a parallel manner, there are no dependencies between them.

#### 4.5. Action Anticipation on EPIC-Kitchens

Tab. 7 shows the performance comparison for the action anticipation task on EK55. Top-5 accuracy is measured in each anticipation interval  $\tau_a$ . We also report Top-5 accuracy for verb, noun, and action at the specific anticipation interval 1s. Mean Top-5 recall measures the performance with class-aware properties that are averaged over 26 many-shot verbs, 71 many-shot nouns, and 819 many-shot actions.

With only a single layer deployed, HORST already outperforms many state-of-the-art methods. The accuracy can further boost by stacking two layers instead of using only one layer to have the notable gains.

We observe that our model enjoys a well balanced performance across all the eight anticipation intervals. RL [30] has a better score at the very early stage but cannot maintain its performance on the short anticipation intervals. EL [55], on the other hand, performs strong on shorter anticipation but not with long anticipation. Our model also shows strong Top-5 accuracy for both verb and noun, indicating that spatial-temporal attention is effective in recognizing and tracking the target object already before the target action is observed. The drops between Top-5 accuracy and Mean Top-5 recall may be caused by label imbalance and further amplified by the nature of attention being calculated independently for each sample.

We include RU-LSTM [41] with single RGB branch as the referenced method at the bottom of the table. RU-LSTM is a highly specialized design for the egocentric action anticipation task, with an additional recurrent layer to unroll the

last layer predictions over the anticipation interval till reaching the starting time of target action. Our model is slightly under-performing when compared to RU-LSTM. However, our proposed method is a general design and is orthogonal to their work. Extending HORST with a similar unrolling scheme is a promising direction for future work.

Finally, we report new state of the art accuracy with significant margin to all known competitors in the bottom row of Tab. 7. To obtain this we used a ResNet-50 two-layer HORST architecture and the publicly available action recognition pre-trained weights from EK55 developers [52]. Our performance boost supports the findings from [41] that the observed frames are with insufficient evidences to represent target actions, causing difficulties in training a CNN extractor to provide rich features for aggregated prediction. We observe a large performance boost by pre-training a CNN extractor on frames that are representative of the target actions. Details of this study are provided in the appendix.

## 5. Conclusions

We have presented HORST, Higher Order Recurrent Space-Time Transformer-style architecture for video prediction tasks. Our model is simple, lightweight and has a transparent design. While it achieves state of the art competitive performance on early action recognition and anticipation benchmarks, there is more to explore to optimize it with a task specific design. Competitors explicitly unfold model components over anticipation intervals to predict the future. We will address such extensions in future work.

## Acknowledgments

We gratefully acknowledge the support from Amazon AWS Machine Learning Research Awards (MLRA).



## References

- [1] J. Su, W. Byeon, J. Kossaifi, F. Huang, J. Kautz, and A. Anandkumar, "Convolutional tensor-train LSTM for spatio-temporal learning," in *NeurIPS*, 2020. 1, 2, 6
- [2] A. Furnari and G. M. Farinella, "Rolling-unrolling lstms for action anticipation from first-person video," *IEEE Transactions on Pattern Analysis and Machine Intelligence*, 2020. 1
- [3] Z. Qi, S. Wang, C. Su, L. Su, Q. Huang, and Q. Tian, "Self-regulated learning for egocentric video activity anticipation," *IEEE Transactions on Pattern Analysis and Machine Intelligence*, 2021. 1
- [4] Y. A. Farha and J. Gall, "Uncertainty-aware anticipation of activities," in *ICCV Workshops*, 2019, pp. 1197–1204. 1
- [5] Y. A. Farha, Q. Ke, B. Schiele, and J. Gall, "Long-term anticipation of activities with cycle consistency," *CoRR*, vol. abs/2009.01142, 2020. 1
- [6] G. Bertasius, H. Wang, and L. Torresani, "Is space-time attention all you need for video understanding?" *CoRR*, vol. abs/2102.05095, 2021. 1, 2
- [7] A. Arnab, M. Dehghani, G. Heigold, C. Sun, M. Lucic, and C. Schmid, "ViViT: A video vision transformer," *CoRR*, vol. abs/2103.15691, 2021. 1, 2
- [8] I. Laptev, "On space-time interest points," *International Journal of Computer Vision*, vol. 64, no. 2-3, pp. 107–123, 2005. 2
- [9] H. Wang, A. Kläser, C. Schmid, and C. Liu, "Dense trajectories and motion boundary descriptors for action recognition," *International Journal of Computer Vision*, vol. 103, no. 1, pp. 60–79, 2013. 2
- [10] L. Wang, Y. Xiong, Z. Wang, Y. Qiao, D. Lin, X. Tang, and L. V. Gool, "Temporal segment networks: Towards good practices for deep action recognition," in *ECCV*, 2016. 2
- [11] R. Girdhar, D. Ramanan, A. Gupta, J. Sivic, and B. C. Russell, "Actionvlad: Learning spatio-temporal aggregation for action classification," in *CVPR*, 2017, pp. 3165–3174. 2
- [12] K. Simonyan and A. Zisserman, "Two-stream convolutional networks for action recognition in videos," in *NeurIPS*, 2014, pp. 568–576. 2
- [13] C. Feichtenhofer, A. Pinz, and A. Zisserman, "Convolutional two-stream network fusion for video action recognition," in *CVPR*, 2016, pp. 1933–1941. 2
- [14] D. Tran, L. D. Bourdev, R. Fergus, L. Torresani, and M. Paluri, "Learning spatiotemporal features with 3d convolutional networks," in *ICCV*, 2015, pp. 4489–4497. 2
- [15] J. Carreira and A. Zisserman, "Quo vadis, action recognition? A new model and the kinetics dataset," in *CVPR*, 2017, pp. 4724–4733. 2
- [16] C. Feichtenhofer, "X3D: expanding architectures for efficient video recognition," in *CVPR*, 2020, pp. 200–210. 2
- [17] D. Tran, H. Wang, L. Torresani, J. Ray, Y. LeCun, and M. Paluri, "A closer look at spatiotemporal convolutions for action recognition," in *CVPR*, 2018, pp. 6450–6459. 2
- [18] J. Lin, C. Gan, and S. Han, "TSM: temporal shift module for efficient video understanding," in *ICCV*, 2019, pp. 7082–7092. 2
- [19] S. Sudhakaran, S. Escalera, and O. Lanz, "Gate-shift networks for video action recognition," in *CVPR*, 2020, pp. 1099–1108. 2
- [20] D. Tran, H. Wang, M. Feiszli, and L. Torresani, "Video classification with channel-separated convolutional networks," in *ICCV*, 2019, pp. 5551–5560. 2
- [21] Y. Li, B. Ji, X. Shi, J. Zhang, B. Kang, and L. Wang, "TEA: temporal excitation and aggregation for action recognition," in *CVPR*, 2020, pp. 906–915. 2
- [22] Y. Meng, R. Panda, C. Lin, P. Sattigeri, L. Karlinsky, K. Saenko, A. Oliva, and R. Feris, "Adafuse: Adaptive temporal fusion network for efficient action recognition," *CoRR*, vol. abs/2102.05775, 2021. 2
- [23] Z. Li, K. Gavriluyk, E. Gavves, M. Jain, and C. G. M. Snoek, "Videolstm convolves, attends and flows for action recognition," *Computer Vision and Image Understanding*, vol. 166, pp. 41–50, 2018. 2
- [24] R. Girdhar and D. Ramanan, "Attentional pooling for action recognition," in *NeurIPS*, 2017, pp. 34–45. 2
- [25] S. Sudhakaran, S. Escalera, and O. Lanz, "LSTA: long short-term attention for egocentric action recognition," in *CVPR*, 2019, pp. 9954–9963. 2
- [26] A. Vaswani, N. Shazeer, N. Parmar, J. Uszkoreit, L. Jones, A. N. Gomez, L. Kaiser, and I. Polosukhin, "Attention is all you need," in *NeurIPS*, 2017, pp. 5998–6008. 2
- [27] R. Girdhar, J. Carreira, C. Doersch, and A. Zisserman, "Video action transformer network," in *CVPR*, 2019, pp. 244–253. 2
- [28] X. Wang, R. B. Girshick, A. Gupta, and K. He, "Non-local neural networks," in *CVPR*, 2018, pp. 7794–7803. 2
- [29] Y. Chen, Y. Kalantidis, J. Li, S. Yan, and J. Feng, "A<sup>2</sup>-nets: Double attention networks," in *NeurIPS*, 2018, pp. 350–359. 2
- [30] S. Ma, L. Sigal, and S. Sclaroff, "Learning activity progression in lstms for activity detection and early detection," in *CVPR*, 2016, pp. 1942–1950. 2, 8
- [31] M. S. A. Akbarian, F. Saleh, M. Salzmann, B. Fernando, L. Petersson, and L. Andersson, "Encouraging lstms to anticipate actions very early," in *ICCV*, 2017, pp. 280–289. 2
- [32] Y. Kong, Z. Tao, and Y. Fu, "Deep sequential context networks for action prediction," in *CVPR*, 2017, pp. 3662–3670. 2
- [33] R. D. Geest and T. Tuytelaars, "Modeling temporal structure with LSTM for online action detection," in *WACV*, 2018, pp. 1549–1557. 2, 8
- [34] Y. Wang, L. Jiang, M. Yang, L. Li, M. Long, and L. Fei-Fei, "Eidetic 3d LSTM: A model for video prediction and beyond," in *ICLR*, 2019. 2, 6
- [35] K. M. Kitani, B. D. Ziebart, J. A. Bagnell, and M. Hebert, "Activity forecasting," in *ECCV*, 2012, pp. 201–214. 3

- [36] H. S. Koppula and A. Saxena, "Anticipating human activities using object affordances for reactive robotic response," *IEEE Transactions on Pattern Analysis and Machine Intelligence*, vol. 38, no. 1, pp. 14–29, 2016. [3](#)
- [37] C. Vondrick, H. Pirsiavash, and A. Torralba, "Anticipating visual representations from unlabeled video," in *CVPR*, 2016, pp. 98–106. [3](#)
- [38] J. Gao, Z. Yang, and R. Nevatia, "RED: reinforced encoder-decoder networks for action anticipation," in *BMVC*, 2017. [3](#), [8](#)
- [39] Y. A. Farha, A. Richard, and J. Gall, "When will you do what? - anticipating temporal occurrences of activities," in *CVPR*, 2018, pp. 5343–5352. [3](#)
- [40] A. Miech, I. Laptev, J. Sivic, H. Wang, L. Torresani, and D. Tran, "Leveraging the present to anticipate the future in videos," in *CVPR Workshops*, 2019, pp. 2915–2922. [3](#)
- [41] A. Furnari and G. M. Farinella, "What would you expect? anticipating egocentric actions with rolling-unrolling lstms and modality attention," in *ICCV*, 2019, pp. 6251–6260. [3](#), [5](#), [8](#), [11](#)
- [42] Z. Qi, S. Wang, C. Su, L. Su, Q. Huang, and Q. Tian, "Self-regulated learning for egocentric video activity anticipation," *IEEE Transactions on Pattern Analysis and Machine Intelligence*, 2021. [3](#), [11](#)
- [43] C. Yu, X. Ma, J. Ren, H. Zhao, and S. Yi, "Spatio-temporal graph transformer networks for pedestrian trajectory prediction," in *ECCV*, 2020, pp. 507–523. [3](#)
- [44] Y. Dong, J.-B. Cordonnier, and A. Loukas, "Attention is not *all* you need: Pure attention loses rank doubly exponentially with depth," *CoRR*, vol. abs/2103.03404, 2021. [5](#)
- [45] R. Goyal, S. E. Kahou, V. Michalski, J. Materzynska, S. Westphal, H. Kim, V. Haenel, I. Fründ, P. Yianilos, M. Mueller-Freitag, F. Hoppe, C. Thureau, I. Bax, and R. Memisevic, "The "something something" video database for learning and evaluating visual common sense," in *ICCV*, 2017, pp. 5843–5851. [5](#)
- [46] D. Damen, H. Doughty, G. M. Farinella, S. Fidler, A. Furnari, E. Kazakos, D. Moltisanti, J. Munro, T. Perrett, W. Price *et al.*, "Scaling egocentric vision: The epic-kitchens dataset," in *ECCV*, 2018, pp. 720–736. [5](#), [8](#)
- [47] A. Furnari, S. Battiato, and G. Maria Farinella, "Leveraging uncertainty to rethink loss functions and evaluation measures for egocentric action anticipation," in *ECCV Workshops*, 2018. [5](#), [8](#)
- [48] S. Ioffe and C. Szegedy, "Batch normalization: Accelerating deep network training by reducing internal covariate shift," in *ICML*, 2015, pp. 448–456. [5](#)
- [49] E. D. Cubuk, B. Zoph, J. Shlens, and Q. V. Le, "Randaugment: Practical automated data augmentation with a reduced search space," in *CVPR Workshops*, 2020, pp. 702–703. [5](#)
- [50] J. Zhuang, T. Tang, Y. Ding, S. C. Tatikonda, N. C. Dvornek, X. Papademetris, and J. S. Duncan, "Adabelief optimizer: Adapting stepsizes by the belief in observed gradients," in *NeurIPS*, 2020. [5](#)
- [51] M. Zhang, J. Lucas, J. Ba, and G. E. Hinton, "Lookahead optimizer: k steps forward, 1 step back," in *NeurIPS*, vol. 32, 2019. [5](#)
- [52] W. Price and D. Damen, "An evaluation of action recognition models on epic-kitchens," *CoRR*, vol. abs/1908.00867, 2019. [8](#), [11](#)
- [53] C. Vondrick, H. Pirsiavash, and A. Torralba, "Anticipating visual representations from unlabeled video," in *CVPR*, 2016, pp. 98–106. [8](#)
- [54] L. Berrada, A. Zisserman, and M. P. Kumar, "Smooth loss functions for deep top-k classification," in *ICLR*, 2018. [8](#)
- [55] A. Jain, A. Singh, H. S. Koppula, S. Soh, and A. Saxena, "Recurrent neural networks for driver activity anticipation via sensory-fusion architecture," in *ICRA*, 2016, pp. 3118–3125. [8](#)
- [56] Y. Wu, L. Zhu, X. Wang, Y. Yang, and F. Wu, "Learning to anticipate egocentric actions by imagination," *IEEE Transactions on Image Processing*, vol. 30, pp. 1143–1152, 2020. [11](#)
- [57] S. Sudhakaran, S. Escalera, and O. Lanz, "Learning to recognize actions on objects in egocentric video with attention dictionaries," *IEEE Transactions on Pattern Analysis and Machine Intelligence*, 2021. [11](#)

## A. Details on Multi-Label Prediction

In EK55 each *action* is described by the composition of a *noun* and a *verb*. To take into account such label structure both in prediction and for learning, we follow the "multi-head prediction" three branches design of [57].

We use three classifiers, one for *verb*, one for *noun*, and one for *action*, having parameters  $\theta_{verb}, \theta_{noun}, \theta_{action}$ . Each classifier is *avg-pool* followed by a fully-connected layer, with input  $h(t)$  for *noun*,  $st-Att(t)$  for *verb*, and the concatenated  $[h(t), st-Att(t), y(t)]$  for *action*. (recall Fig. 3 and Eq. (1) and (4) of main paper).

During training, the overall loss function is jointly optimized over the three provided class labels  $l_v, l_n, l_a$  using

$$\begin{aligned} L_{verb} &= \mathbb{1}_v \cdot \log\text{-prob}(st\text{-Att}(t); \theta_{verb}) \\ L_{noun} &= \mathbb{1}_n \cdot \log\text{-prob}(h(t); \theta_{noun}) \\ L_{action} &= \mathbb{1}_a \cdot \log\text{-prob}([h(t), st\text{-Att}(t), y(t)]; \theta_{action}) \\ L_{overall} &= \alpha L_{verb} + \beta L_{noun} + \gamma L_{action} \end{aligned}$$

where  $\mathbb{1}_*$  is the binary indicator of label  $l_*$ . We used  $\alpha = \beta = \gamma = 1$  for all the experiments throughout this work.

## B. Additional Results on EPIC-Kitchens

In Tab. 9 we include a performance analysis of HORST on EK55 Action Anticipation using different backbones and pre-training strategies. For these we (i) followed the precise implementation and training protocol of Sec. 4.2 of main paper, and (ii) used the pre-trained weights made available from the dataset developers at <https://github.com/epic-kitchens/epic-kitchens-55-action-models>. This analysis reveals that HORST realizes state of the art performance with large margin to all previously best performing methods, see Tab. 8. Please note that we use RGB-only to outperform competitors that use flow and object features in addition to RGB.

## C. Additional Visualizations

We provide additional examples of spatial-temporal attention visualization on SSv2 in Fig. 5 and EK55 in Fig. 6.

## C.1. Examples from Something-Something

Fig. 5a shows an example with correct prediction "*Pouring [something] into [something]*". Notice the top-right changes from the spatial attention and the border of the glass cup successfully capture the *pouring* action and the position of the cup, which provide a clear hint to the model for making the precise choice. (please note there exists another category with label "*Pouring [something] out of [something]*").

Fig. 5b highlights the relative position on the spatial maps of two objects and triggers a correct prediction. The background is ignored in the spatial attention map, which shows the capability of filtering irrelevant features even when the background is with a distracting pattern. Also, temporal attention focuses on the older frames. This may be due to the fact that the action is already happening early in the clip and no relevant changes are observed in the last eight frames.

Fig. 5c shows a mis-classified example due to lack of observation frames. The prediction turns from "*[Something] falling like a feather or paper*" to "*Holding [something]*" without observing the *falling* action.

Fig. 5d is another example with incorrect prediction because of lacking observations. Even a human may find these two examples difficult to early predict the action, without providing more evidence. Not observing subsequent frames turns the predicted action from *falling* to *holding* while missing the guess about whether the object will be rolling or not. It is worth noting that the last example is with more temporal weighting on the frames when the object touches the surface, which plays a crucial role leading to the reasonable prediction.

## C.2. Examples from EPIC-Kitchens

Fig. 6 shows some visualizations of spatial-temporal attentions and compares ground-truth label with top-5 model predictions at 1s anticipation interval. We used the TSN pre-trained ResNet-50 based HORST model from row 5 in Table 9 for these visualizations. Spatial attentions are performed on the 8x14 ResNet-50 feature maps for EK55, as opposed to 56x56 used in SSv2, and are upscaled to input resolution 256x454. Coarse-grained features, but with

	Methods	Top-5 Accuracy % at different $\tau_a$								Top-5 Acc. % @ 1s			Mean Top-5 Rec. % @ 1s		
		2	1.75	1.5	1.25	1.0	0.75	0.5	0.25	Verb	Noun	Action	Verb	Noun	Action
Multimodal	RU [41]	29.44	30.73	32.24	33.41	35.32	36.34	37.37	38.98	79.55	51.79	35.32	43.72	49.90	<b>15.10</b>
	SRL [42]	30.15	31.28	32.36	34.05	35.52	36.77	38.60	40.49	-	-	-	-	-	-
	ImagineRNN [56]	-	-	32.50	33.60	35.60	36.70	38.50	39.40	-	-	-	-	-	-
RGB only	RU [41]	25.44	26.89	28.32	29.42	30.83	32.00	33.31	34.47	-	-	30.83	-	-	-
	SRL [42]	25.82	27.21	28.52	29.81	31.68	33.11	34.75	36.89	78.90	47.65	31.68	42.83	47.64	13.24
	HORST (BNInc, [41])	25.38	26.37	27.82	29.16	30.69	31.54	32.52	33.45	77.67	46.34	30.69	36.54	44.33	10.94
	HORST (ResNet50, [52])	<b>30.81</b>	<b>32.22</b>	<b>33.31</b>	<b>34.55</b>	<b>36.56</b>	<b>38.23</b>	<b>39.08</b>	<b>41.43</b>	<b>80.19</b>	<b>54.79</b>	<b>36.56</b>	<b>45.26</b>	<b>55.01</b>	13.90

Table 8: EPIC-Kitchens Action Anticipation results.

Table 9: EPIC-Kitchens Action Anticipation results comparison of HORST with different backbones.

Pretrain Arch.	Base	Top-5 Accuracy % at different $\tau_a$								Top-5 Acc. % @ 1s			Mean Top-5 Rec. % @ 1s		
		2	1.75	1.5	1.25	1.0	0.75	0.5	0.25	Verb	Noun	Action	Verb	Noun	Action
from Table 7		25.38	26.37	27.82	29.16	30.69	31.54	32.52	33.45	77.67	46.34	30.69	36.54	44.33	10.94
TSN	BNInception	28.88	29.40	30.63	32.06	33.29	34.55	35.72	37.91	79.71	51.31	33.29	42.27	50.43	12.48
TRN	BNInception	27.09	28.24	29.28	30.87	32.70	33.63	35.08	36.56	79.63	50.06	32.70	41.09	50.07	11.95
MTRN	BNInception	27.63	28.42	29.67	31.86	33.27	34.37	36.22	38.01	79.47	50.24	33.27	43.05	49.95	12.47
TSN	ResNet50	30.81	32.22	33.31	34.55	36.56	38.23	39.08	41.43	80.19	54.79	36.56	45.26	55.01	13.90
TRN	ResNet50	29.22	30.23	31.30	32.98	34.65	35.76	37.77	39.04	79.44	52.49	34.65	42.76	51.70	12.80
MTRN	ResNet50	29.63	30.83	32.22	33.41	35.24	36.75	38.03	40.25	80.35	52.76	35.24	45.20	52.54	13.91

higher semantic meaning, are observed compared to the spatial maps shown in Fig. 5.

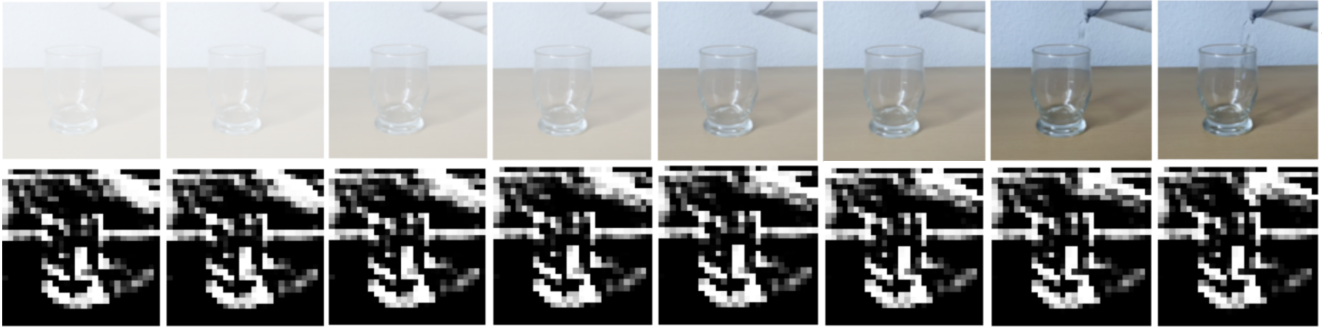
Fig. 6a is an example video clip with anticipation label *Take Spatula*. We can find the objects *spoon* and *spatula* appear at different times in the video clip. The *spatula* is being blocked (occluded) in the frame that has got the largest temporal attention weighting, which leads to a wrong top-1 prediction with a guess on *spoon* instead of *spatula*.

Fig. 6b is a sample with the target label *Open Oil*. From the predictions we can see the model is pretty confident about the interacting object *oil*. But the uncertainty of the hand movement also reflects on the diverging choices over the verbs.

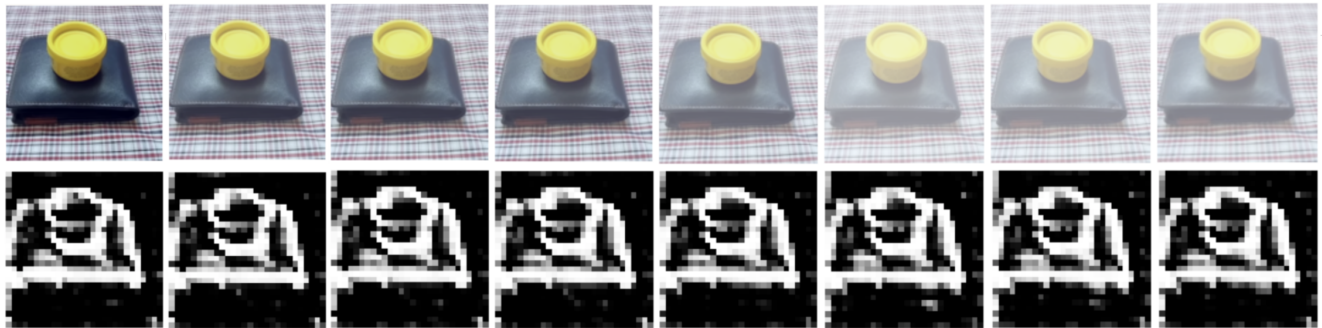
Fig. 6c shows an example with correct prediction on *Wash Board*. By observing the changes of temporal attention weighting, the model stops referencing the recent inputs once it has a confident prediction. Spatial attention also spots the target action correctly.

Fig. 6d shows a challenging example with the anticipation label *Throw Onion*. We can see the model struggles on the nouns, between *onion* and *skin*, as it is not observing entirely onion in any frame. Although the spatial-temporal attention produced a reasonable spotting area on hand, and focuses on those frames where the participant moved in the scene, the top-5 predictions still failed to meet the ground-truth by the limited information revealed in the video.

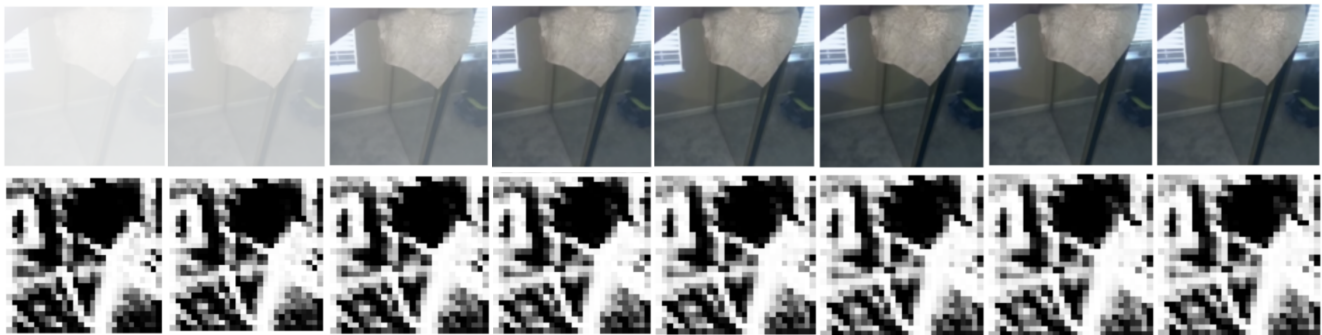




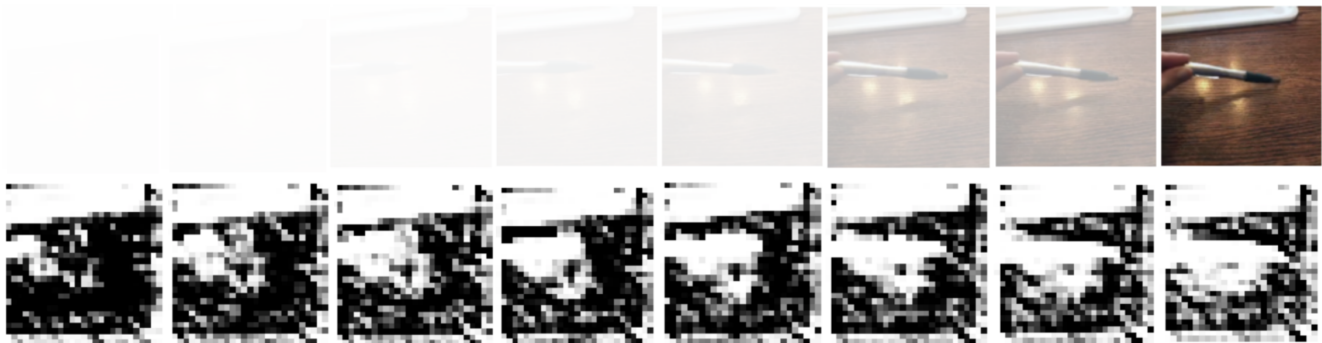
(a) **GT:** Pouring [something] into [something]. **PR:** Pouring [something] into [something]. (✓)



(b) **GT:** Showing [something] on top of [something]. **PR:** Showing [something] on top of [something]. (✓)



(c) **GT:** [Something] falling like a feather or paper. **PR:** Holding [something]. (✗)

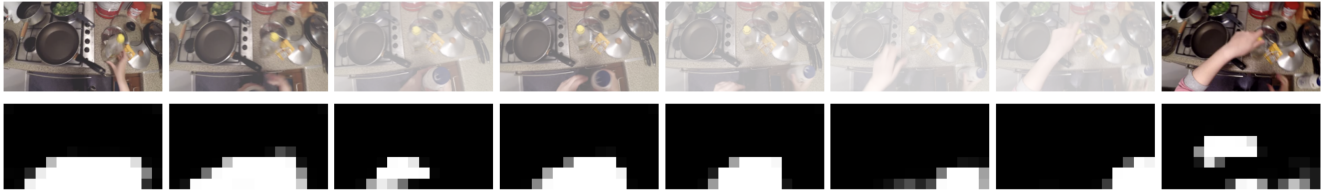


(d) **GT:** Putting [something] on a flat surface without letting it roll. **PR:** Putting [something] on a surface. (✗)

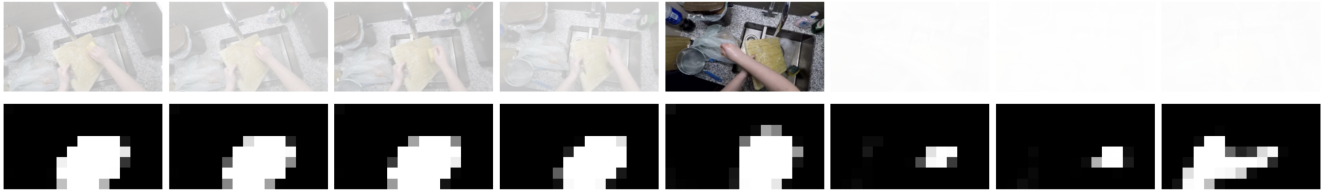
Figure 5: Visualization of spatial-temporal attention on SSv2. These additional examples contain two correctly predicted examples and two mis-classified examples. The horizontal axis contains 8 frames ordered by the occurrence time from left to right. Each example comes with two rows: the upper rows are the input frames weighted by  $\mathcal{T}$ ; the bottom rows show the corresponding  $\mathcal{S}$  maps. The caption of each figure reveals its ground-truth label and predictions.



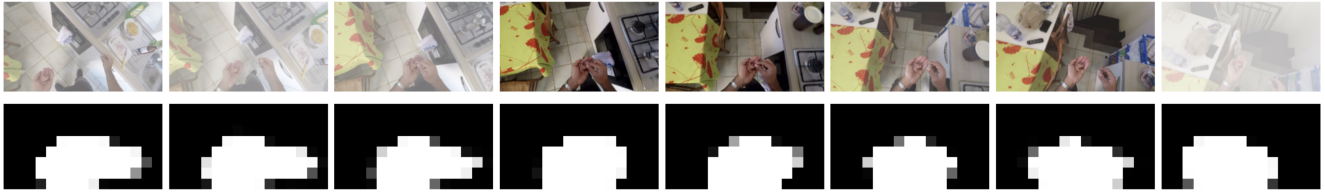
(a) GT: Take Spatula; Top-5 PR: Take Spoon, Take Spatula, Put Cup, Take Cup, Put Plate



(b) GT: Open Oil; Top-5 PR: Put-Down Oil, Take Oil, Open Door, Pour Oil, Open Oil



(c) GT: Wash Board; Top-5 PR: Wash Board, Put-Down Board, Turn-Off Tap, Put-Down Sponge, Stir Pan



(d) GT: Throw Onion; Top-5 PR: Open Door, Throw Skin, Take Onion, Take Skin, Take-Off Skin

Figure 6: Visualization of spatial-temporal attention on EK55. The horizontal axis contains 8 frames ordered by the occurrence time from left to right, the last frame is at 1s of anticipation interval. Each example comes with two rows: the upper rows are the input frames weighted by  $\mathcal{T}$ ; the bottom rows show the corresponding  $\mathcal{S}$  maps. The caption of each figure reveals its ground-truth (verb, noun) pair and top-5 predictions.